Thermal Science and Engineering 2026, 9(2), 6075.
https://doi.org/10.24294/tse6075

Article

MHD natural convection flow in a vertical channel in the presence of point/line heat source/sink under third-kind thermal boundary conditions

Basant K. Jha[1], Muhammad M. Altine[2]*

[1] Department of Mathematics, Ahmadu Bello University Zaria, Kaduna State, P.M.B. 1045, Nigeria;
[2] Department of Mathematics, Federal University Birnin Kebbi, Kebbi State, P.M.B. 1157, Nigeria;
* **Corresponding author:** Muhammad M. Altine, altine@fubk.edu.ng

CITATION

Jha B K., Altine, M M. MHD natural convection flow in a vertical channel in the presence of point/line heat source/sink under third-kind thermal boundary conditions. Thermal Science and Engineering. 2026; 9(2): 6075.
https://doi.org/10.24294/tse6075

ARTICLE INFO

Received: 29 April 2024
Accepted: 25 May 2026
Available online: 16 June 2026

Abstract: This research considers the impact of a point/line heat source/sink on steady magnetohydrodynamic (MHD) natural convection flows in a vertical channel subjected to a transverse magnetic field with a thermal boundary condition of the third-kind thermal (Robin) boundary conditions. A constant point/line heat source/sink generates convection current within the flow. The governing dimensional equations regulating the physical situation at hand are presented in dimensionless form with the associated boundary conditions. Exact solutions are derived for the momentum and energy equations using the Laplace transform technique. The effects of key controlling parameters involved in flow formations are studied, such as the magnetic parameter, point/line heat source/sink parameter and Biot number on flow behaviour are analyzed. MATLAB software is employed to obtain line graphical and tabular results. The findings indicate that lower values of the Biot number account for reduced heat transfer to the surroundings, whilst higher values lead to higher surface heat transfer. Furthermore, the heat transfer rate, frictional drag force and mass flow rate retard as the line heat source/sink approaches a point heat source. In addition, the mass flow rate increases by almost 49% as the interval between the line heat source increases. for both equal and unequal values of the Biot number. There is remarkable agreement between the current results and the previously published studies.

Keywords: third-kind thermal boundary conditions; natural convective flow; line heat source; point heat source

1. Introduction

The thermal boundary condition of the third kind (Robin boundary condition) arises in many heat transfer scenarios and is frequently encountered in a wide range of applications, including heat exchangers, electronic component cooling, and geothermal systems. This boundary condition is critical in determining the heat transfer rate and temperature distributions, as it is based on Newton's law of cooling. According to Javeri [1], this condition occurs during the heat transfer process when radiative heat transfer is present at the channel wall. Prakash and Muthtamilselvan [2] analyzed the influence of third-kind thermal boundary conditions and viscous dissipation on laminar, fully developed mixed convection flow in a vertical channel. The study examined external fluids under both scenarios of symmetric and asymmetric reference temperatures. They found that perturbation and mixed convection parameters improved the flow domain, whereas viscosity ratio, ratio width ratio, and conductivity ratio suppressed it.

Davis and Breneri [3] developed a theoretical model that described the effect of Robin boundary conditions in two insulated adjacent rough channels. Ajibade and

Muhammad [4] presented a theoretical analysis of time-dependent natural convection Couette flow with wall conduction under Robin boundary conditions. Additional studies addressing the impact of third-kind thermal boundary conditions can be found in [5–7].

Numerous researchers have also explored the magnetic field influence in the flow realm under various configurations and orientations [8–11]. This concept has been widely applied in power generation systems, particularly in the design of magnetohydrodynamic (MHD) generators. The use of MHD extends to cancer tumor treatment, magnetotherapy, gastrointestinal issues, magnetic endoscopy, and MRI in biology, geophysics, and medicine. Sparrow and Cess [12] found that although magnetic fields have minimal impact on other fluids, they significantly affect the buoyancy-induced liquid metal's natural convection heat transfer. Khanafer and Chamkha [13] discovered that the intensity and angle of the magnetic field had a critical bearing on the movements of heat and fluid through the angled barrier. A strong magnetic field applied to a porous material dramatically reduced convective current. Furthermore, the combination of a magnetic field and a porous substance created a tricky situation for the flow of heat and fluids in the medium. Sheikholeslami et al. [14] explored the function of a plate fluctuating vertically through a porous medium with an unsteady MHD flow of a nanofluid that was both electrically conductive and radiating. Dwivedi et al. [15] investigated the fully developed viscous and electrically conducting fluid on free convection flow exposed to a transverse magnetic field in an infinitely fixed vertical plate. They examined the outcome for both symmetric and asymmetric heating of the region's vertically oriented walls in open and closed circuit configurations. The investigation found that the long-circuit setup had a more resilient induced magnetic field, induced current and velocity than the short-circuit layout. Other significant studies on magnetohydrodynamics and heat transfer can be found in [16–21].

When examining fluid flow, integration of a heat source/sink is crucial. These variables significantly influence the ultimate product's structure and quality; in the same way, the heat source/sink approach has a profound impact on the circulation of temperature throughout the fluid. The influence of heat source/sink significantly to analyzing the function of the brain in neuroscience. Some of the research that highlights the heat source/sink function on mixed convection fluid flow includes [22–29], where different physical conditions were considered. However, the preceding studies did not examine the role of the line/point heat source/sink. The effects of these parameters in fluid mechanics are critical scientific phenomena that aid in the diminution and augmentation of flow formation. Dwivedi and Singh [30,31] studied the role of a point heat source on an induced magnetic field in an upstanding channel and cylinder, respectively. Similarly, Jha et al. [32] examined the impact of point/line heat sources on natural convection flow. The consequences of a point/line heat source induce free convection in the working fluid, as in many real-world operations. Other evaluated material includes [33–35].

Recently, Jha et al., [36] employed the Laplace transform technique to study the impact of point/line heat source/sink together with suction/injection on MHD natural convection flow. The results demonstrate that increasing the suction/injection parameter decreases the mass flow rate by 8.9%. Also, increasing the magnetic

parameter strength leads to a mass flow rate drop by almost 27%. In another development, the impact of thermal radiation, the soret, buoyancy, and the addition of suction/injection phenomena driven by point/line heat source arrangement were examined by Parasuraman and Begum [37]. According to the study's results, the rate of mass transfer noticeably increases as the Soret effect gets stronger.

Although extensive investigations have been carried out on the influence of the third-kind thermal boundary conditions on steady natural convection flow of an electrically conducting, viscous and incompressible fluid in vertically arranged plates, most existing literature focuses on constant heat source/sink or simplified boundary conditions such as Dirichlet (isothermal) or Neumann cases. Studies that incorporate third-kind thermal boundary conditions have improved the physical realism of the thermal modelling by accounting for convective heat exchange at the boundaries. However, these investigations predominantly assume a constant heat source/sink, which does not adequately represent localized thermal disturbances encountered in practical systems such as cooling of electric components, geothermal systems and heat exchangers.

This research aims to combine the influence of the third-kind thermal boundary conditions on steady natural convection flow of an electrically conducting, viscous and incompressible fluid in vertically arranged plates in the presence of a transverse magnetic field, incorporating the point/line heat source/sink. The Laplace transform method is used to obtain a closed-form solution of the modified, non-dimensional leading equations. There is remarkable consistency between the numerical values and graphical results of the current studies and the work of [35] for large values of the Biot number. The current results of this study can help in the mitigation and enhancement of flow formation caused by line and point heat sources.

2. Mathematical analysis

A steady, fully developed free convection laminar flow of a viscous, incompressible, and electrically conducting fluid across two infinite vertical channel walls of distance L apart (see **Figure 1**). A uniform transverse magnetic field is applied perpendicular to the plates along $y-$ axis with a point/line source/sink, it is considered. Following the work of Dwivedi et al. [35], a point or line heat source/sink creates heat in the fluid subject to the third-kind thermal boundary conditions, resulting in free convection of the working fluid. The direction of the fluid flow is taken on the $x-$ axis in the vertical direction, while on the contrary, the $y-$ axis is horizontally perpendicular to the walls.

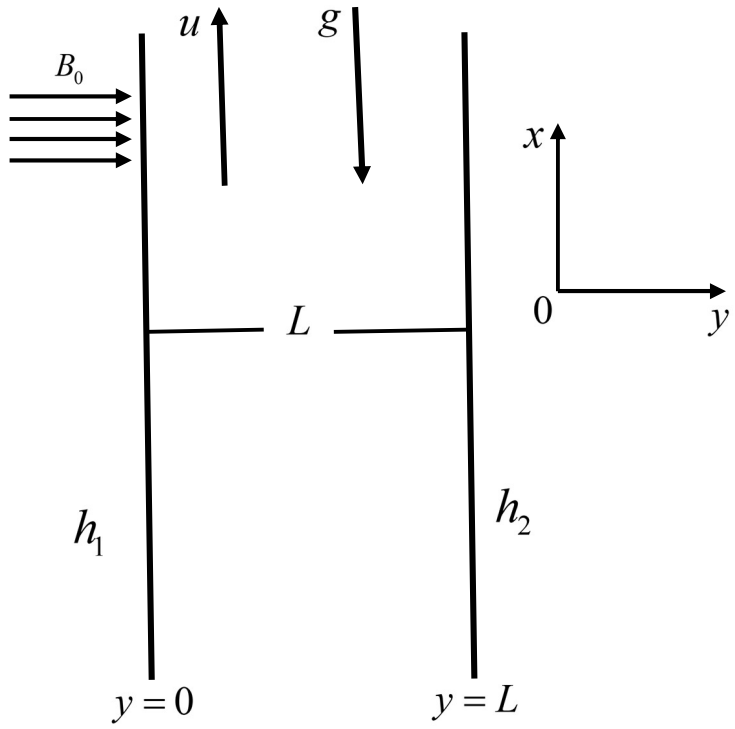

Figure 1. geometry of the problem.

Using the Wavelet function $F\left(y,a',b'\right)$ for the point/line heat source/sink formulation, which is given by Dwivedi et al. [35] as:

$$F\left(y,\,a',\,b'\right)=H\left(y-a'\right)-H\left(y-b'\right)=\begin{cases}0,\ y<a'\\ L,\ a'<y<b'\\ 0,\ y>b'\\ \dfrac{1}{2},\ y=a'\ \text{or}\ y=b'\end{cases}, \tag{1}$$

The arbitrary variables a' and b' ranging between 0 and L, specified as $0<a'<b'<L$ are used. The function (1) functions as a point source/sink if the distance between a' and b' is extremely tiny; otherwise, it functions as a line source/sink.

The leading equations under the usual Boussinesq approximation are as follows, after taking into consideration the point/line heat source/sink as proposed by Dwivedi et al., [35]:

$$\upsilon\frac{d^2u}{dy^2}-\frac{\sigma B_0^2}{\rho}u+g\beta\left(T-T_c\right)=0 \tag{2}$$

$$k\frac{d^2T}{dy^2}+Q_0F\left(y,a',b'\right)=0. \tag{3}$$

and, the model's boundary conditions are as follows:

$$u = 0,\ -k\frac{dT}{dy} = h_1\left(T_c - T\right) \text{ at } y = 0, \tag{4}$$

$$u = 0,\ -k\frac{dT}{dy} = h_2\left(T - T_c\right) \text{ at } y = L. \tag{5}$$

After introducing the dimensionless variables described by [35], the dimensionless version of **Equations (2)** to **(5)** may be obtained.

$$U = \frac{u}{U_0}, \qquad Y = \frac{y}{L}, \qquad U_0 = \frac{g\beta L^2 T_c}{\upsilon}, \qquad \theta = \frac{T - T_c}{T_c}, \qquad a = \frac{a'}{L}, \quad \text{and} \quad b = \frac{b'}{L}. \tag{6}$$

Equations (2) and **(3)** may be expressed in their dimensionless form using the dimensionless values in **Equation (6)**:

$$\frac{d^2U}{dY^2} - M^2U + \theta = 0 \tag{7}$$

$$\frac{d^2\theta}{dY^2} + SF\left(Y, a, b\right) = 0 \tag{8}$$

where $S = Q_0 L / kT_c$ is a heat source/sink parameter, $M = B_0 L\sqrt{\sigma / \mu}$ is the magnetic parameter, $Bi_1 = h_1 L / k$ and $Bi_2 = h_2 L / k$ are the Biot numbers. The dimensionless formulation for the point/line heat source/sink is as follows:

$$F\left(Y, a, b\right) = H\left(Y - a\right) - H\left(Y - b\right) = \begin{cases} 0, & Y < a \\ 1, & a < Y < b \\ 0, & Y > b \\ \dfrac{1}{2}, & Y = a \text{ or } Y = b \end{cases} \quad \text{with } 0 < a < b < 1. \tag{9}$$

The boundary conditions **(4)** and **(5)** in non-dimensional forms are:

$$U = 0,\ \frac{d\theta}{dY} = Bi_1\theta \text{ at } Y = 0 \tag{10}$$

$$U = 0,\ \frac{d\theta}{dY} = -Bi_2\theta \text{ at } Y = 1. \tag{11}$$

In the dimensionless process, the property of the unit step functions $H\left(yL\right) = \dfrac{H\left(y\right)}{\left|L\right|}$ is used.

To get the expression of **Equations (7)** and **(8)** subject to **(10)** and **(11)**, the researchers employed the Laplace transform (L.T) approach defined:

$$F(s)=\int_0^{\infty} f(Y)e^{-sy}dY, \tag{12}$$

where $F(s)$ represents the Laplace transform $f(Y)$ and s is the Laplace parameter defined as $s>0$.

The results of the velocity and temperature expressions are:

$$\begin{aligned} U(Y)=&\frac{\sinh(MY)}{M}\begin{bmatrix} x_1\left(2(b-a)+Bi_2\left(a^2-b^2-2(a-b)\right)\right) \\ -S\left(\frac{1}{M^4}\begin{pmatrix}\cosh(M(1-a)) \\ -\cosh(M(1-b))\end{pmatrix}-\frac{1}{2M^2}\left(a^2+b^2-2a\right)\right)\end{bmatrix} \\ &-x_2\left[2(b-a)+Bi_2\left(a^2-b^2-2(a-b)\right)\right] \\ &+S\begin{bmatrix} -\frac{1}{2M^2}\left(H(Y-a)(Y-a)^2-H(Y-b)(Y-b)^2\right) \\ +\frac{1}{M^4}\begin{pmatrix}H(Y-a)\cosh(M(Y-a))-H(Y-b)\cosh(M(Y-b)) \\ -H(Y-a)+H(Y-b)\end{pmatrix}\end{bmatrix}\end{aligned} \tag{13}$$

$$\begin{aligned}\theta(Y)=&\frac{S(1+Bi_1Y)}{2\left(Bi_1+Bi_2(1+Bi_1)\right)}\left[2(b-a)+Bi_2\left(a^2-b^2-2(a-b)\right)\right] \\ &-\frac{S}{2}\left[H(Y-a)(Y-a)^2-H(Y-b)(y-b)^2\right]\end{aligned} \tag{14}$$

Frictional drag force and heat transfer rate, which describe shear stress and heat transfer coefficients in channel walls, are computed as follows at both walls using **Equations (13)** and **(14)**:

$$\begin{aligned}\tau_0=&\left(\frac{dU}{dY}\right)_{Y=0} \\ =&x_1\left(2(b-a)+Bi_2\left(a^2-b^2-2(a-b)\right)\right) \\ &-S\left(-\frac{1}{2M^2}\left(a^2+b^2-2a\right)+\frac{1}{M^4}\begin{pmatrix}\cosh(M(1-a)) \\ -\cosh(M(1-b))\end{pmatrix}\right)\end{aligned} \tag{15}$$

$$\tau_1 = -\left(\frac{dU}{dY}\right)_{Y=1}$$
$$= \cosh(M)\begin{bmatrix} x_1\left(2(b-a)+Bi_2\left(a^2-b^2-2(a-b)\right)\right) \\ -S\left(\frac{1}{M^4}\begin{pmatrix}\cosh\left(M(1-a)\right) \\ -\cosh\left(M(1-b)\right)\end{pmatrix}-\frac{1}{2M^2}\left(a^2+b^2-2a\right)\right)\end{bmatrix} \quad (16)$$
$$+S\left[-\frac{1}{M^2}\left((b-a)\right)+\frac{1}{M^3}\left(\sinh\left(M(1-a)\right)-\sinh\left(M(1-b)\right)\right)\right]$$
$$-x_3\left[2(b-a)+Bi_2\left(a^2-b^2-2(a-b)\right)\right]$$

$$Nu_0 = \left(\frac{d\theta}{dY}\right)_{Y=0}$$
$$= \frac{SBi_1}{2\left(Bi_1+Bi_2(1+Bi_2)\right)}\left[2(b-a)+a^2-b^2-2(a-b)\right] \quad (17)$$

$$Nu_1 = -\left(\frac{d\theta}{dY}\right)_{Y=1}$$
$$= \frac{SBi_1}{2\left(Bi_1+Bi_2(1+Bi_2)\right)}\left[Bi_1\left(a^2-b^2-2(a-b)\right)\right] \quad (18)$$

Following the work of Jha et al. [32] integrating **Equation (13)** yields the expression for the mass flow rate as follows:

$$Q = \int_0^1 U dY$$
$$= \frac{\left(\cosh(M)-1\right)}{M^2}\begin{bmatrix} x_1\left(2(b-a)+Bi_2\left(a^2-b^2-2(a-b)\right)\right) \\ -S\left(+\frac{1}{M^4}\begin{pmatrix}\cosh\left(M(1-a)\right) \\ -\cosh\left(M(1-b)\right)\end{pmatrix}-\frac{1}{2M^2}\left(a^2+b^2-2a\right)\right)\end{bmatrix} \quad (19)$$
$$-x_4\left[2(b-a)+Bi_2\left(a^2-b^2-2(a-b)\right)\right]$$
$$+S\left[-\frac{1}{6M}\left((1-a)^3-(1-b)^3\right)+\frac{1}{M^5}\begin{pmatrix}\sinh\left(M(1-a)\right)-\sinh\left(M(1-b)\right) \\ -M\left((1-a)+(1-b)\right)\end{pmatrix}\right.$$

where x_1, x_2, x_3 and x_4 are arbitrary constants defined in the **Appendix**.

3. Result and discussion

Graphical representations for velocity (U) and temperature (θ) distributions and tabular expressions for frictional drag force, heat transfer rate and mass flow rate using a MATLAB R2016a program are presented and discussed under various

pertinent parameters. The results present the impact of the constant point/line heat source/sink, magnetic parameter (M) and Biot number $(Bi_1 \text{ and } Bi_2)$ on the velocity and temperature profiles.

Dwivedi et al.'s [35] research is used as a benchmark solution to validate the accuracy of the present work by comparing the numerical values of the heat transfer rate, frictional drag force, and mass flow rate. It is confirmed from **Table 1** that the results agree with the findings of Dwivedi et al. [35]. For large values of the Biot numbers $(Bi_1 = Bi_2 \to \infty)$, similarly, it is noticed from **Figure 2a,b**, that the current study is in good harmony with the work of [35] for large values of Biot number for both cases of point and line heat sources.

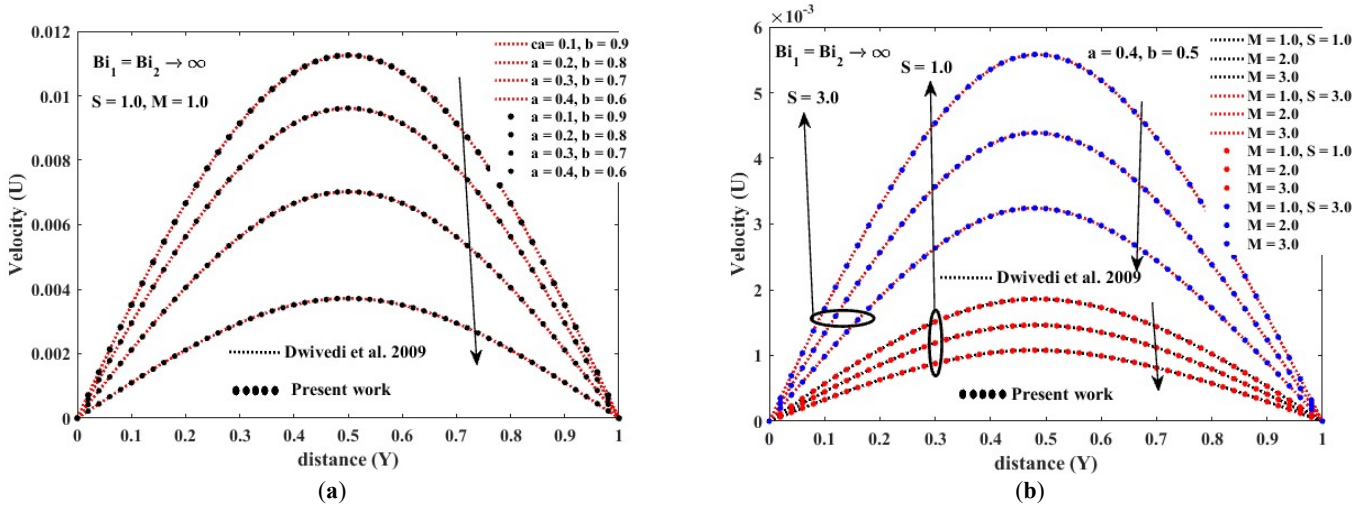

Figure 2. (a) variation of line heat source parameter on the velocity profile for fixed values of M and S Bi_1 and Bi_2. (b) variation of M and S near the center of channel walls. For large values of Bi_1 and Bi_2.

Figure 3 depicts the impacts of point/line heat source, magnetic (M), and a constant heat source (S) parameters on the velocity (U) profiles for equal values of the Biot number $Bi_1 = Bi_2$. The Figure shows that when the magnetic parameter (M) strength increases, the fluid velocity profile slows down. This is because an increase in the magnetic parameter creates a resistive force similar to the drag force acting in the opposite direction of the fluid, causing the velocity to drop. On the other hand, increasing the value of the heat source parameter improves the velocity distribution. Furthermore, as the line heat source approaches the point heat source, the velocity retards. This is due to the fact that a line heat source produces a stronger convection current in comparison to a point heat source.

In **Figure 4**, the influence of constant heat source and a line heat source on the temperature distribution is plotted for an equal value of Biot number. It is observed from the Figure that when the Biot number values remain the same at both channel walls, the temperature profile remains symmetric near the channel center. It is noticed that the line heat source is characterised by producing higher internal heat energy than the point heat source, causing the temperature of the fluid to grow. Similarly,

increasing the value of the S tends to enhance the fluid temperature. An increase in the convection current accompanies this behaviour.

Figure 5 is associated with the impacts of M , S and point/line heat sources on the velocity profile near the edges of the channel walls, for equal values of the Biot number. As mentioned in **Figure 1** above, a surge in the magnetic parameter reduces the velocity due to the action of the Lorenz force. Conversely, an increase in the S yields a correlating increase in the fluid velocity, as seen in **Figure 5**. It is revealed from the Figure that an increase in the heat source parameter near the left wall amplifies fluid flow near the left wall and vice versa.

The effect of S on the temperature fields for equal values of Biot number near the center of the channel are depicted in **Figure 6** for given values of a and b . It is apparent from the Figure that a rise in the value of S increases the fluid temperature profile. This is due to the fact that the heat source effect provides a strong convection current and hence increases the temperature. This behaviour illustrates that the thermal energy within the fluid is directly proportional to the magnitude of the constant heat source.

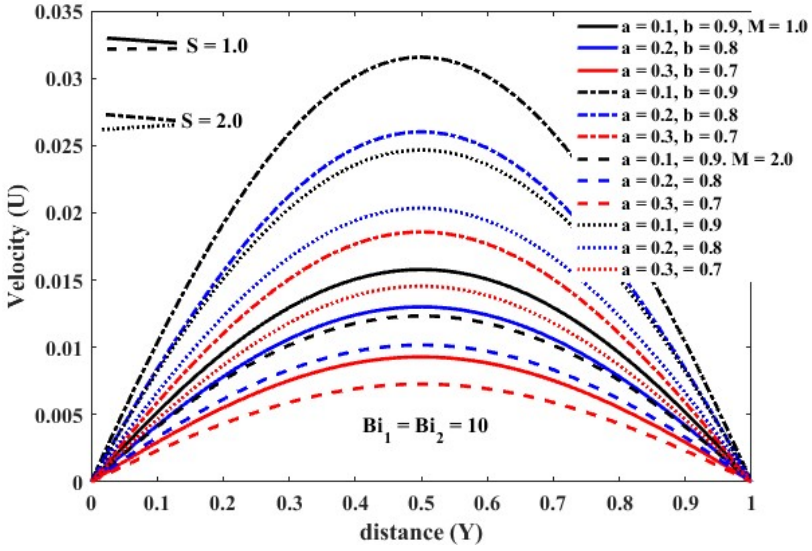

Figure 3. variation of M, S and line heat sourceon velocity profiles for equal Biot number.

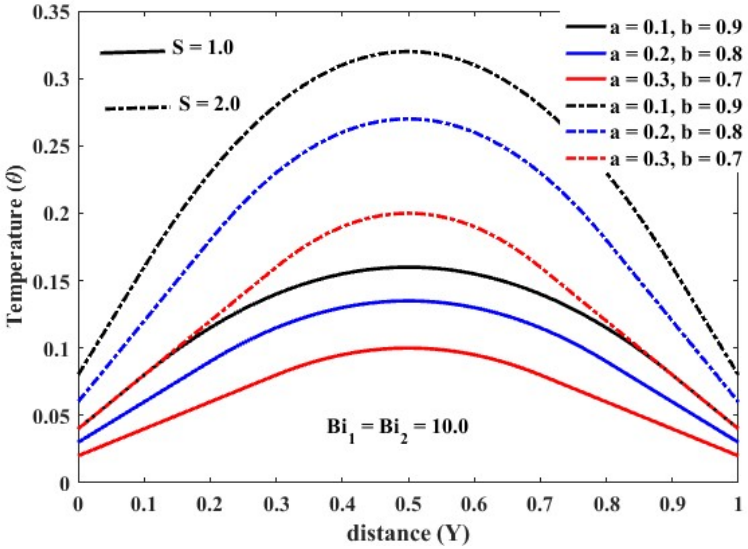

Figure 4. variation of M, S and line heat source on temperature profiles for equal Biot number.

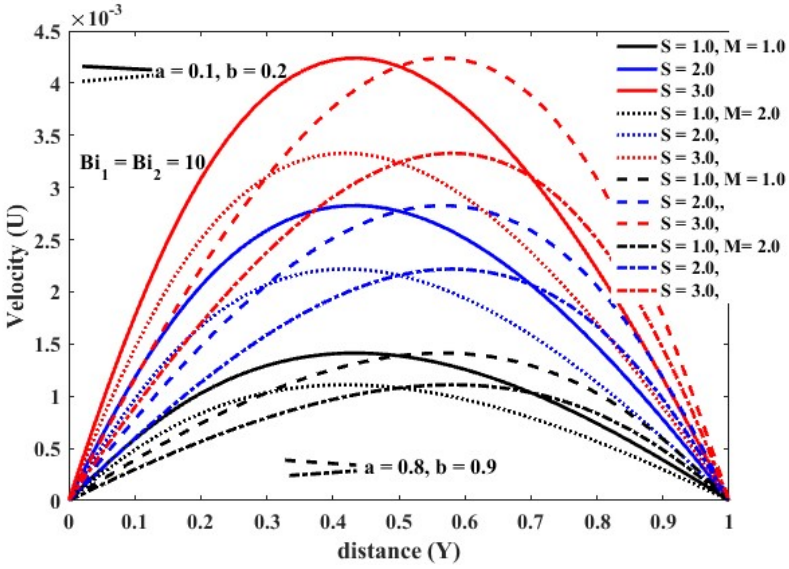

Figure 5. variation of M and S on velocity profile for equal Biot number in the case of point heat source near both channel walls.

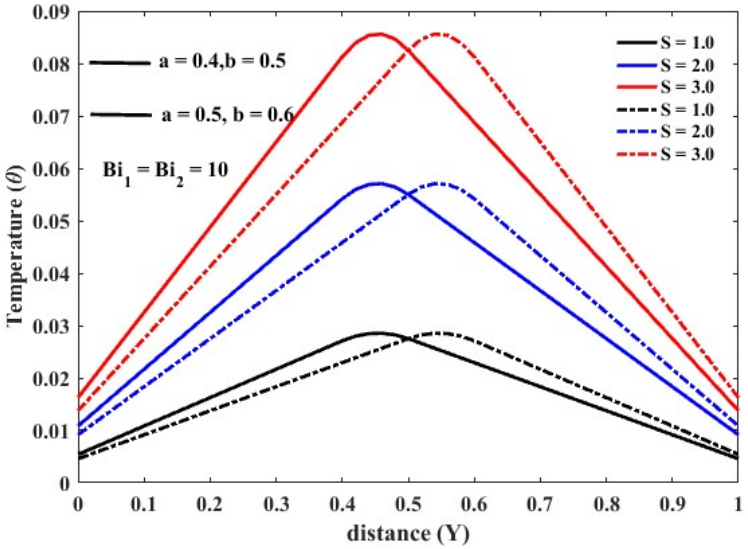

Figure 6. variation of M and S on temperature profiles for equal Biot number in case of point heat source near the center of the channel walls.

Figure 7 describes the behaviour of the velocity profile with the key parameter in the governing equations for unequal values of the Biot number $Bi_1 > Bi_2$. The velocity distribution decreases as the gap between the line heat source decreases. It is found that fluid velocity varies inversely as the magnitude of the magnetic parameter increases. This could be attributed to the fact that Lorenz force generation by the applied transverse magnetic field, which acts to the opposite direction of the fluid motion. **Figure 7** further shows the role of Biot number, the velocity profile exhibits a noticeable enhancement, this is due to the increases convective heat exchange at the channel walls, which enhances the thermal interaction between the fluid and its surroundings. This behaviour is further confirmed in **Figure 8** for $Bi_1 < Bi_2$

Figure 9 plots the dimensionless temperature profile for $Bi_1 > Bi_2$ for different values of a, b and S. It is interesting to observe that the temperature at each location in the channel is an increasing function of the line heat source. However, the impact Biot number on temperature is stronger near the right wall of the channel. This can be attributed to the fact that an unequal Biot number introduces asymmetry in the thermal field, resulting in a non-uniform temperature distribution. Similar trend is observed in **Figure 10** when $Bi_1 < Bi_2$. An increase in the temperature profile is directly proportional to the Biot number, as a result of enhanced thermal interaction at the boundaries.

The plots of velocity variation for $Bi_1 = 10.0$ and $Bi_2 = 1.0$ for various values of M and S are displayed in **Figure 11**. It is observed that as the point heat source increases to a line heat source, the velocity increases. Also, by increasing the heat source parameter, the fluid flow enhances. The effect of $Bi_1 > Bi_2$ is higher near the right wall due to heat accumulation on that wall. It is noticed from **Figure 11** that the velocity variation at each location is a decreasing function of M. The pattern is also

confirmed in **Figure 12**, the velocity tilted toward the channel wall with a higher Biot number.

Figure 13 depicts the effect of the heat source parameter on the temperature profile in the case of the point heat source at the edges of the channel walls for $Bi_1 > Bi_2$. The temperature at both walls is an increasing function of S. However, as $Bi_1 = 10.0$ and $Bi_2 = 1.0$, the temperature on the right wall increases rapidly due to heat accumulation at that wall. Consequently, a reverse trend is observed in **Figure 14**, as $Bi_1 = 1.0$ and $Bi_2 = 10.0$, the temperature is more pronounced at the left wall $Y = 0$.

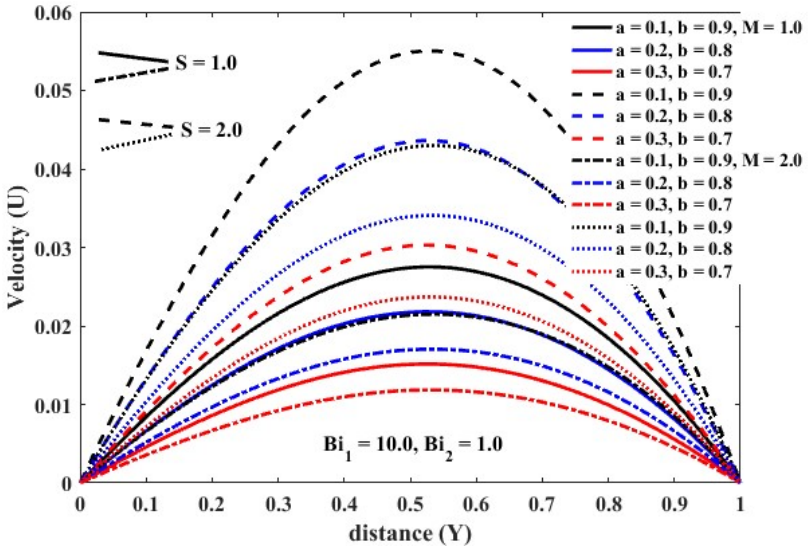

Figure 7. variation of M and S on velocity profile for $Bi_1 = 10.0$, $Bi_2 = 1.0$ in the case of line heat source.

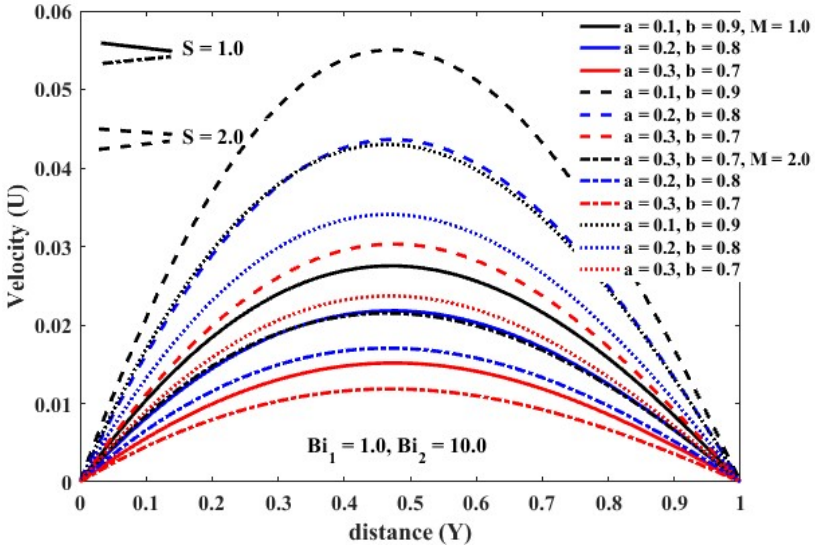

Figure 8. variation of M and S on velocity profile for $Bi_1 = 1.0$, $Bi_2 = 10.0$ in the case of line heat source.

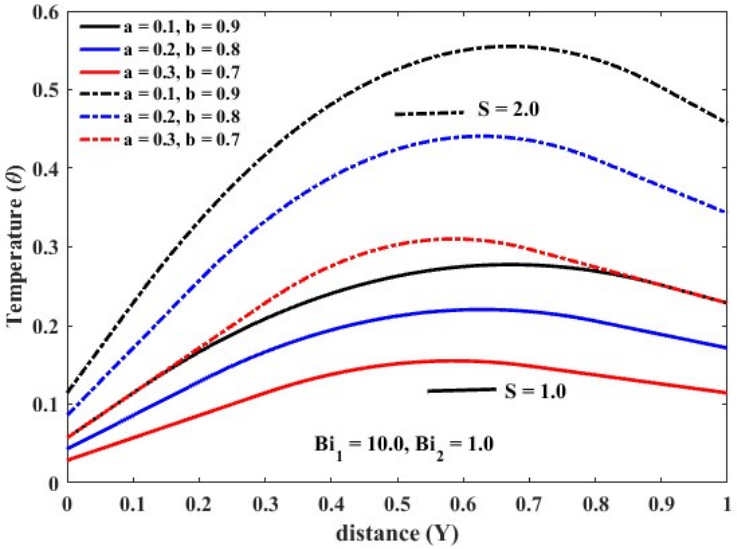

Figure 9. variation of M and S on temperature profiles for $Bi_1 = 10.0,\ Bi_2 = 1.0$ in the case of line heat source.

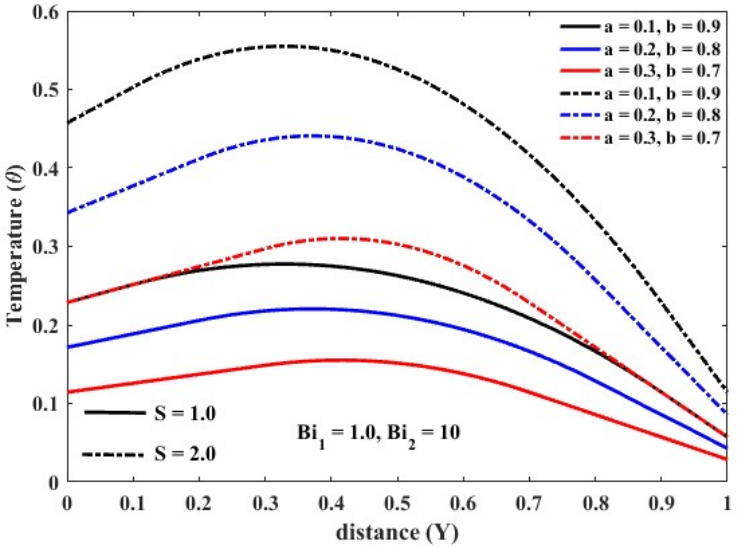

Figure 10. variation of M and S on temperature profile for $Bi_1 = 1.0,\ Bi_2 = 10.0$ in the case of line heat source.

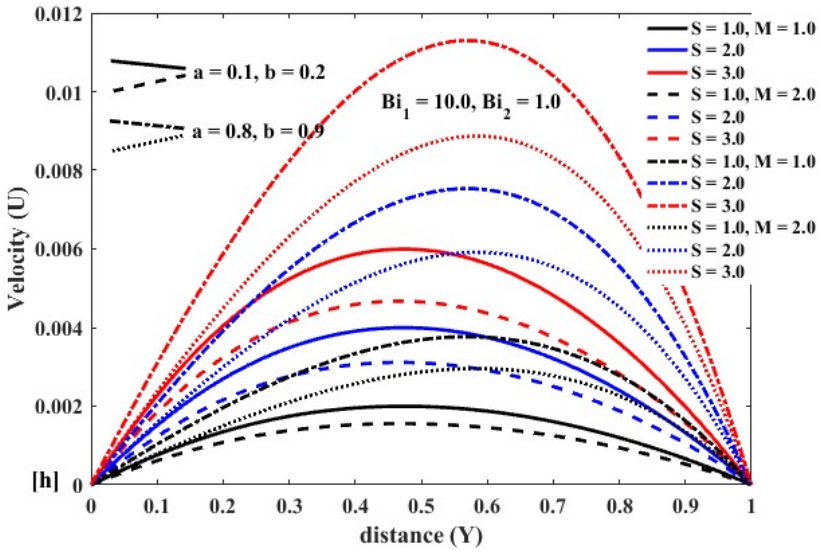

Figure 11. variation of M and S on velocity profile $Bi_1 = 10.0,\ Bi_2 = 1.0$ in the case of point heat source near both channel walls.

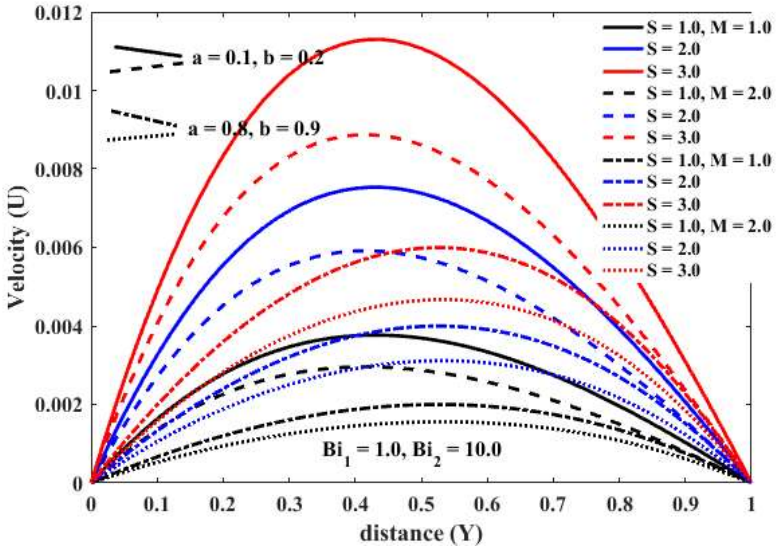

Figure 12. variation of M and S on velocity profile for $Bi_1 = 1.0,\ Bi_2 = 10.0$ in the case of point heat source near the edges channel walls.

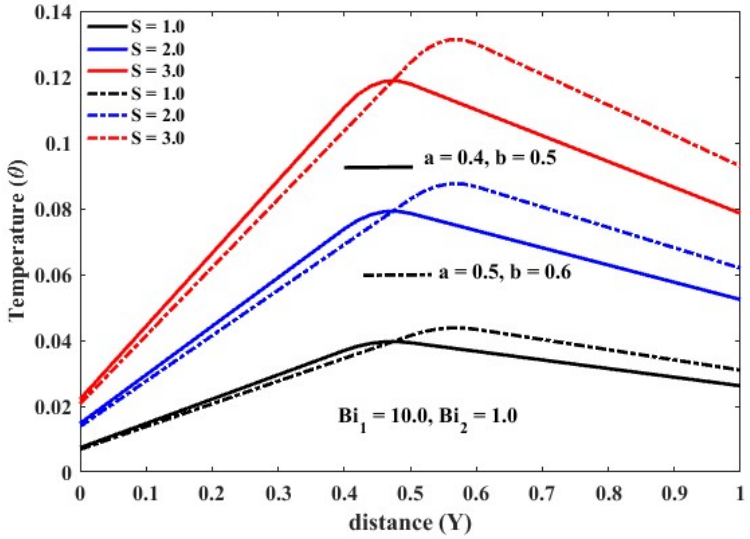

Figure 13. variation of M and S on temperature profile for $Bi_1 = 10.0,\ Bi_2 = 1.0$ in the case of point heat source near the center of the channel walls.

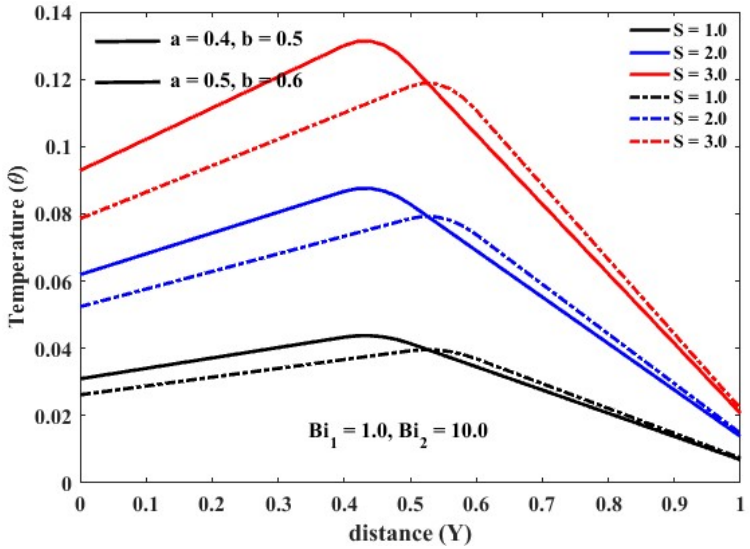

Figure 14. variation of M and S on temperature profiles for $Bi_1 = 1.0,\ Bi_2 = 10.0$ near the center of the channel walls.

Table 2 displays the heat transfer rate, frictional drag force, and mass flow rate for the selected arbitrary values of the point/line heat source, constant heat source and magnetic parameters (M). Equal and unequal values of Biot numbers are considered. The table demonstrates that for equal values of Biot numbers ($Bi_1 = Bi_2 = 10.0$), the numerical values of the heat transfer rate at both walls $\left(Nu_0 \text{ and } Nu_1\right)$, frictional force $\left(\tau_0 \text{ and } \tau_1\right)$, and mass flow rate $\left(Q\right)$ retard near the edges of the channel walls for both cases of point and line heat sources. On the other hand, the heat transfer rate decreases near the channel wall (Y = 0) in the case of a point heat source and increases near the channel wall (Y = 1). For $Bi_1 < Bi_2$, it is observed that the heat transfer rate,

frictional drag force, and mass flow rate are decreasing functions of the point/line heat source. However, it is observed that when $Bi_1 < Bi_2$, the heat transfer rate value is higher at the right wall compared to the left wall. This is physically true because the lower values of Biot number lead to weak convective heat exchange, accounting for a lower heat transfer rate, whilst the higher values lead to stronger heat exchange with the surroundings, resulting to higher surface heat transfer. Also, the frictional drag force values are more assertive near the left wall with respect to the right. furthermore, from the table, it is noticed that the heat transfer rate, frictional drag force, and mass flow rate decrease with decreasing values of line heat source intervals for $Bi_1 > Bi_2$. The heat transfer rate is stronger at the right wall, whilst the opposite trend is observed for the frictional drag force, which is higher at the left wall $Bi_1 > Bi_2$. The mass flow rate is a decreasing function for both equal and unequal values of Biot numbers.

Table 1. Computations for Nusselt numbers $\left(Nu_{(0,1)}\right)$, skin frictions $\left(\tau_{(0,1)}\right)$ near the two vertical walls and the mass flow rate (Q) in the presence of a point/line heat source, showing comparison for Dwivedi *et al*., [35] results when Bi_1 and Bi_2 are very large for a fixed value of $M = 1.0$.

S	a	b	**Dwivedi *et al.*, [35]**					**Present work**				
			Nu_0	Nu_1	τ_0	τ_1	Q	Nu_0	Nu_1	τ_0	τ_1	Q
1.0	0.1	0.9	0.40000	0.40000	0.03570	0.03570	0.007200	0.40000	0.40000	0.03570	0.03570	0.007200
	0.3	0.7	0.20000	0.20000	0.02150	0.02150	0.004400	0.20000	0.20000	0.02150	0.02150	0.004400
	0.4	0.6	0.10000	0.10000	0.01120	0.01120	0.002300	0.10000	0.10000	0.01120	0.01120	0.002300
	0.10	0.11	0.00890	0.00110	0.00028	0.00015	0.000039	0.00890	0.00110	0.00028	0.00015	0.000039
	0.20	0.21	0.00790	0.00210	0.00045	0.00029	0.000072	0.00790	0.00210	0.00045	0.00029	0.000072
	0.80	0.81	0.00200	0.00800	0.00028	0.00044	0.000069	0.00200	0.00800	0.00028	0.00044	0.000069
	0.90	0.91	0.00095	0.00900	0.00014	0.00025	0.000035	0.00095	0.00900	0.00014	0.00025	0.000035
2.0	0.1	0.9	0.80000	0.80000	0.07150	0.07150	0.014400	0.80000	0.80000	0.07150	0.07150	0.014400
	0.3	0.7	0.40000	0.40000	0.04290	0.04290	0.008900	0.40000	0.40000	0.04290	0.04290	0.008900
	0.4	0.6	0.20000	0.20000	0.02230	0.02230	0.004700	0.20000	0.20000	0.02230	0.02230	0.004700
	0.10	0.11	0.01790	0.00210	0.00055	0.00031	0.000078	0.01790	0.00210	0.00055	0.00031	0.000078
	0.20	0.21	0.01590	0.00410	0.00090	0.00059	0.000014	0.01590	0.00410	0.00090	0.00059	0.000014
	0.80	0.81	0.00390	0.01610	0.00056	0.00087	0.000014	0.00390	0.01610	0.00056	0.00087	0.000014

	0.90	0.91	0.00190	0.01810	0.00028	0.00051	0.00007 1	0.00190	0.01810	0.00028	0.00051	0.00007 1

Table 2. Nusselt numbers $\left(N_{u(0,1)}\right)$, skin frictions $\left(\tau_{(0,1)}\right)$ and mass flow rate $\left(Q\right)$ near the two vertical walls in case of a point/line heat source for different values of Biot numbers $\left(Bi\right)$ for fixed values of $M=1.0$ and $S=1.0$.

Bi_1	Bi_2	a	b	Nu_0	Nu_1	τ_0	τ_1	Q
10	10	0.1	0.9	0.400000	0.400000	0.054222	0.054222	0.064239
		0.3	0.7	0.200000	0.200000	0.030694	0.030694	0.032954
		0.4	0.6	0.100000	0.100000	0.015791	0.015791	0.016588
		0.10	0.11	0.008292	0.001708	0.000561	0.000332	0.001197
		0.20	0.21	0.007458	0.002542	0.000721	0.000484	0.001117
		0.80	0.81	0.002458	0.007542	0.000470	0.000709	0.000439
		0.90	0.91	0.001625	0.008375	0.000316	0.000540	0.000293
10	20	0.1	0.9	0.382609	0.417391	0.050825	0.047974	0.061100
		0.3	0.7	0.191304	0.208696	0.028996	0.027570	0.031384
		0.4	0.6	0.095652	0.104348	0.014942	0.014229	0.015803
		0.10	0.11	0.008217	0.001783	0.000547	0.000305	0.001183
		0.20	0.21	0.007348	0.002652	0.000700	0.000444	0.001097
		0.80	0.81	0.002130	0.007820	0.000406	0.000591	0.000379
		0.90	0.91	0.001261	0.008739	0.000245	0.000410	0.000227
20	10	0.1	0.9	0.417391	0.382609	0.047974	0.050825	0.037615
		0.3	0.7	0.208696	0.191304	0.027580	0.028996	0.019642
		0.4	0.6	0.104348	0.095652	0.014229	0.014942	0.009932
		0.10	0.11	0.008652	0.001348	0.000432	0.000262	0.000645
		0.20	0.21	0.007783	0.002217	0.000605	0.000421	0.000620
		0.80	0.81	0.002565	0.007435	0.000431	0.000688	0.000275
		0.90	0.91	0.001696	0.008304	0.000291	0.000527	0.000185

From **Table 3**, it is observed that, for equal values of the Biot number, the mass flow rate increases by 49.18% when the point heat source is transformed into a line heat source. It also increases by 6.68% near the left wall. On the other hand, the mass flow rate increases by 33.26%.

Furthermore, for $Bi_1 < Bi_2$, the mass flow rate increases by 49.14% as the interval between the line heat source increases. Similarly, the mass flow rate increases by 7.27% and 40.11% near the left and right walls, respectively.

Moreover, as $Bi_1 > Bi_2$, the mass flow rate increases by 48.61%. In addition, increases of 3.88% and 32.73% are observed near the left and right walls, respectively.

The percentage is obtained using the formula $\left(\left(\frac{(\text{line heat source} - \text{point heat source})}{\text{line heat source}}\right)*100\right)$.

Table 3. shows the percentage decrease in mass flow rate for different values of Biot number and point/line heat source.

Bi_1	Bi_2	a	b	Q	Q %
10	10	0.1	0.9	0.064239	48.7009
		0.3	0.7	0.032954	49.6632
		0.4	0.6	0.016588	
		0.10	0.11	0.001197	6.68338
		0.20	0.21	0.001117	
		0.80	0.81	0.000439	33.2574
		0.90	0.91	0.000293	
10	20	0.1	0.9	0.061100	48.6350
		0.3	0.7	0.031384	49.6463
		0.4	0.6	0.015803	
		0.10	0.11	0.001183	7.26965
		0.20	0.21	0.001097	
		0.80	0.81	0.000379	40.1055
		0.90	0.91	0.000227	
20	10	0.1	0.9	0.037615	47.7815
		0.3	0.7	0.019642	49.4349
		0.4	0.6	0.009932	
		0.10	0.11	0.000645	3.87597
		0.20	0.21	0.000620	
		0.80	0.81	0.000275	32.7273
		0.90	0.91	0.000185	

4. Conclusion

An exact solution of steady free convection flow of electrically conducting, viscous, incompressible fluid in the presence of a transverse magnetic field in a vertical channel caused by a point/line heat source/sink under third-kind thermal boundary conditions is revealed. The Laplace transform method is used to solve the governing equations analytically. The exact expressions for the velocity and temperature profiles, mass flow rate, frictional drag force (at both channel walls), and Nusselt number are determined. Comparisons with existing literature are conducted. The influence of controlling parameters on the velocity and temperature profiles is presented with the help of line graphs, and the numerical values of the heat transfer rate, frictional factor at both channel walls and mass flux rate are tabulated. Based on the results acquired, the following observations are established:

1. The lower values of the Biot number lead to weak convective heat exchange, accounting for a lower heat transfer rate, whilst the higher values lead to stronger heat exchange with the surroundings, resulting in higher surface heat transfer.
2. The velocity and temperature distributions have higher values for the line heat source relative to the point heat source for equal and unequal values of the Biot number.
3. The heat transfer rate, frictional drag force and mass flow rate retards as the line heat source approaches a point heat source.
4. The velocity and temperature profiles are increasing functions of a constant heat source.
5. A rise in the magnetic parameter values reduces the flow of the fluid for both cases, with values equal and unequal to the Biot number.
6. The mass flow rate increases by almost 49% as the point heat source is transformed into a line heat source.
7. An increase in mass flow rate is more pronounced near the left wall in comparison to the right wall in the case of point heat, for both equal and unequal values of Biot number.

Nomenclature

Nu_1	Nusselt number at isothermal porous plate
Q_0	heat source/sink volumetric rate (J)
B_0	Constant magnetic field
S	Constant heat generation parameter
g	acceleration due to gravity (m/s^2)
L	difference between the porous plates (m)
u	velocity of the fluid in x the direction (m/s)
U	dimensionless velocity
u_0	characteristic velocity of the fluid (m/s)
T	temperature of the fluid (K)
T_c	temperature of isothermal porous plate (K)
C_p	specific heat at constant pressure (KJ/kgK)
$h_{1,2}$	convection heat transfer coefficients at both walls.
σ	Electrical conductivity

Greek Letters

β	Thermal expansion Coefficient (K^{-1})
k	thermal conductivity (w/mk)
μ	fluid Kinematic viscosity (m^2/s)
ρ	fluid density (Kg/m^2)
$\tau_{(0,1)}$	dimensionless skin friction at the porous plates $(y = 0, y = l)$
υ	kinematic viscosity (m^2/s)
θ	dimensionless temperature of the fluid

Conflict of Interest: The authors declare that they have no conflict of interest.

References

1. Javeri V. Laminar heat transfer in a rectangular channel for the temperature boundary condition of the third kind. International Journal of Heat and Mass Transfer. 1978;21(8):1029-1034.
2. Prakash D, Ragupathi E, Muthtamilselvan M, Abdalla B, Mdallal QMA. Impact of boundary conditions of third kind on nanoliquid flow and Radiative heat transfer through asymmetrical channel. Case Studies in Thermal Engineering. 2021;28:101488. doi:10.1016/j.csite.2021.101488
3. Davis AMJ, Brenner H. Use of boundary conditions of the third kind to model heat conduction between two proximate rough surfaces separated by an insulator. International journal of heat and mass transfer. 1997;40(6):1459-1465.
4. Ajibade A, Muhammad A. Steady natural convection Couette flow with wall conduction and thermal boundary condition of third kind. ZAMM Journal of applied mathematics and mechanics: Zeitschrift für angewandte Mathematik und Mechanik. 2020;100:18. doi:10.1002/zamm.201900095
5. Colbrook MJ, Ayton LJ, Fokas AS. The unified transform for mixed boundary condition problems in unbounded domains. Proceedings of the Royal Society A. 2019;475(2222):20180605.
6. Song L, Li PW, Gu Y, Fan CM. Generalized finite difference method for solving stationary 2D and 3D Stokes equations with a mixed boundary condition. Computers & Mathematics with Applications. 2020;80(6):1726-1743. doi:10.1016/j.camwa.2020.08.004
7. Vendin S V. Calculation of nonstationary heat conduction in multilayer objects with boundary conditions of the third kind. Journal of Engineering Physics and Thermophysics. 1993;65(2):823-825. doi:10.1007/BF00861548
8. El Koumy SR, Barakat ESI, Abdelsalam SI. Hall and Porous Boundaries Effects on Peristaltic Transport Through Porous Medium of a Maxwell Model. Transport in Porous Media. 2012;94(3):643-658. doi:10.1007/s11242-012-0016-y
9. Mekheimer K, Komy S, Abdelsalam S. Simultaneous effects of magnetic field and space porosity on compressible Maxwell fluid transport induced by a surface acoustic wave in a microchannel. Chinese Physics B. 2013;22:124702. doi:10.1088/1674-1056/22/12/124702
10. Abdelsalam SI, Bhatti MM. The study of non-Newtonian nanofluid with hall and ion slip effects on peristaltically induced motion in a non-uniform channel. RSC Advances. 2018;8(15):7904-7915. doi:10.1039/C7RA13188G
11. Abdelsalam SI, Bhatti MM. The impact of impinging TiO nanoparticles in Prandtl nanofluid along with endoscopic and variable magnetic field effects on peristaltic blood flow. Multidiscipline Modeling in Materials and Structures. 2018;14(3):530-548. doi:10.1108/MMMS-08-2017-0094
12. Sparrow EM, Cess RD. The effect of a magnetic field on free convection heat transfer. International Journal of Heat and Mass Transfer. 1961;3(4):267-274. doi:10.1016/0017-9310(61)90042-4
13. Khanafer KM, Chamkha AJ. Hydromagnetic natural convection from an inclined porous square enclosure with heat generation. Numerical Heat Transfer, Part A Applications. 1998;33(8):891-910.
14. Sheikholeslami M, Gorji-Bandpay M, Ganji DD. Magnetic field effects on natural convection around a horizontal circular cylinder inside a square enclosure filled with nanofluid. International Communications in Heat and Mass Transfer. 2012;39(7):978-986. doi:10.1016/j.icheatmasstransfer.2012.05.020
15. Dwivedi N, Singh AK, Chandran P, Sacheti NC. Hydromagnetic free convection in a vertical channel with induced magnetic field: Open and short circuits. Pramana—Journal of Physics. 2022;96:99.
16. Mahreen A, Mebarek-Oudina F, Ashfaq A, Raza J, Khan SU, Vaidya H. MHD Thermosolutal Flow in Casson-Fluid Microchannels: Taguchi--GRA--PCA Optimization. Fluid Dynamics & Materials Processing. 2025;21(11):2829.
17. Gambo D, Gambo JJ. Role of suction/injection and slip flow on hydromagnetic free convective flow in a vertical coaxial cylinder under the influence of radial magnetic field. Heat Transfer. 2021;50(5):4775-4787.
18. Zeeshan, Ahammad NA, Shah NA, Chung JD, Khan MS. Computational and Stability Analysis of MHD Time-Dependent Thermal Reaction Flow Impinging on a Vertical Porous Plate Enclosing Magnetic Prandtl Number and Thermal Radiation Effect. Mathematics. 2023;11(6):1376.
19. Jha BK, Gambo D. Hydrodynamic behaviour of velocity of applied magnetic field on unsteady MHD Couette flow of dusty fluid in an annulus. The European Physical Journal Plus. 2022;137(1):67.
20. Yellamma, Narayanappa M, Udhayakumar R, Almarri B, Ramakrishna S, Elshenhab AM. The Impact of Heat Source and Temperature Gradient on Brinkman--Bènard Triple-Diffusive Magneto-Marangoni Convection in a Two-Layer System. Symmetry. 2023;15(3):644.

21. Said BO, Mebarek-Oudina F, Medebber MA. Magneto-hydro-convective nanofluid flow in porous square enclosure. Frontiers in Heat and Mass Transfer. 2024;22(5):1343-1360.
22. Yih KA. Heat source/sink effect on MHD mixed convection in stagnation flow on a vertical permeable plate in porous media. International Communications in Heat and Mass Transfer. 1998;25(3):427-442. doi:10.1016/S0735-1933(98)00030-X
23. Rana P, Bhargava R. Numerical study of heat transfer enhancement in mixed convection flow along a vertical plate with heat source/sink utilizing nanofluids. Communications in Nonlinear Science and Numerical Simulation. 2011;16(11):4318-4334. doi:10.1016/j.cnsns.2011.03.014
24. Umavathi JC, Sheremet MA. Mixed convection flow of an electrically conducting fluid in a vertical channel using Robin boundary conditions with heat source/sink. European Journal of Mechanics - B/Fluids. 2016;55:132-145. doi:10.1016/j.euromechflu.2015.08.013
25. Shashi Prabha GS, Bharathi MC, Kudenatti RB. Heat transfer through mixed convection boundary layer in a porous medium: LTNE analysis. Applied Thermal Engineering. 2020;179:115705. doi:10.1016/j.applthermaleng.2020.115705
26. Taiwo YS, Dauda G. Impact of heat generation/absorption on transient natural convective flow in an annulus filled with porous material subject to isothermal and adiabatic boundaries. GEM - International Journal on Geomathematics. 2019;10(1):20. doi:10.1007/s13137-019-0132-8
27. Hafeez A, Liu D, Ahmad S, Cham BM, Du M, Ahmad S. Three dimensional computational assessments of nano-encapsulated phase change materials: Effects of endothermic and exothermic interactions. International Communications in Heat and Mass Transfer. 2025;169:109801. doi:10.1016/j.icheatmasstransfer.2025.109801
28. Ahmad S, Liu D, Cham BM, Yang S, Sun SL. Exploring conjugate heat transfer in Bingham fluid flow: A 3D computational approach incorporating double diffusion and the Papanastasiou model. Applied Thermal Engineering. 2025;273:126500.
29. Naseem T, Mebarek-Oudina F, Vaidya H, Bibi N, Ramesh K, Khan S. Numerical analysis of entropy generation in joule heated radiative viscous fluid flow over a permeable radially stretching disk. Computer Modeling in Engineering & Sciences. 2025;143(1):351.
30. Dwivedi N, Singh AK. Effect of a Point/Line Heat Source on Hydromagnetic Free Convection between Vertical Walls due to Induced Magnetic Field. Proceedings of the National Academy of Sciences, India Section A: Physical Sciences. 2020. doi:10.1007/s40010-020-00720-x
31. Dwivedi N, Singh AK. Hydromagnetic free convective flow in vertical cylinder due to point/line heat source/sink. Indian Journal of Physics. 2021. doi:10.1007/s12648-021-02193-z
32. Jha BK, Altine M, Hussaini A. Role of Suction/Injection On Free Convective Flow in a Vertical Channel in the Presence of Point/Line Heat Source/Sink. Journal of Heat Transfer. 2022. doi:10.1115/1.4054120
33. Dwivedi N, Singh AK. Effect of line/point heat source and Hall current with induced magnetic field on free convective flow in vertical walls. Indian Journal of Physics. 2021. doi:10.1007/s12648-020-01953-7
34. Dwivedi N, Singh AK. Effect of point/line heat source and Hall current on free convective flow between two vertical walls. Pramana. 2020;94(1):142. doi:10.1007/s12043-020-02009-5
35. Dwivedi N, Singh AK, Kumar A. Natural Convection Between Vertical Walls Due To Point/Line Heat Source/Sink. International Journal of Applied and Computational Mathematics. 2019;5(3):75. doi:10.1007/s40819-019-0659-2
36. Jha BK, Altine MM, Hussaini AM. MHD steady natural convection in a vertical porous channel in the presence of point/line heat source/sink: An exact solution. Heat Transfer. 2023. doi:10.1002/htj.22903
37. Parasuraman L, Begum AM. Point/line heat source configuration with buoyancy and soret effect in a free convective radiative flow over a vertical channel. International Communications in Heat and Mass Transfer. 2024;158:107890. doi:10.1016/j.icheatmasstransfer.2024.107890

Appendix

$$x_1 = \frac{S\left(M^2\left(\cosh\left(M\right)-1\right)+Bi_1\left(\sinh\left(M\right)-1\right)\right)}{2\sinh\left(M\right)\left(Bi_1+Bi_2\left(1+Bi_1\right)\right)M^3} \quad x_2 = \frac{S\left(M\left(\cosh\left(MY\right)-1\right)+Bi_1\left(\sinh\left(MY\right)-MY\right)\right)}{2\left(Bi_1+Bi_2\left(1+Bi_1\right)\right)M^3}$$

$$x_3 = \frac{S\left(M\sinh\left(M\right)+Bi_1\left(\cosh\left(M\right)-1\right)\right)}{2\left(Bi_1+Bi_2\left(1+Bi_1\right)\right)M^2} \qquad x_4 = \frac{S\left(2M\left(\sinh\left(M\right)-M\right)+Bi_1\left(2\cosh\left(M\right)-1\right)\right)}{4\left(Bi_1+Bi_2\left(1+Bi_1\right)\right)M^4}$$